

Slotted Aloha with Capture for OWC-based IoT: Finite Block-Length Performance Analysis

Tijana Devaja, *Student Member, IEEE*, Milica Petkovic, *Member, IEEE*, Francisco J. Escribano, *Senior Member, IEEE*, Čedomir Stefanović, *Senior Member, IEEE*, Dejan Vukobratovic, *Senior Member, IEEE*

Abstract—In this paper, we propose a Slotted ALOHA (SA)-inspired solution for an indoor optical wireless communication (OWC)-based Internet of Things (IoT) system containing IoT devices that exchange data with an access point (AP). Assuming that the OWC receiver at the AP exploits the capture effect, we derive the error probability of decoding a short-length data packet originating from a randomly selected OWC IoT device in the presence of interfering users. The analysis rest on the derivation of the signal-to-noise-and-interference-ratio (SINR) statistics and the application of the finite block-length (FBL) information theory. Using the analytical results, we derive meaningful performance parameters such as system throughput and reliability (expressed in terms of the outage probability of a user transmission). The main trade-offs between the system performance and the OWC system setup parameters are investigated, stressing how the indoor OWC-based system geometry plays an important role in the system performance. Using extensive numerical results, we demonstrate how they can serve as a guideline for a system design aiming at the optimization of the proposed SA-based random access protocol.

Index Terms—Finite Block-Length, Error Probability, Internet of Things, Optical Wireless Communications, Random Access, Slotted ALOHA, Throughput.

I. INTRODUCTION

Optical wireless communications (OWC) have been recently gaining attention as a technology able to offload traffic from wireless radio-frequency (RF) technologies in indoor environments. This may alleviate the challenges posed by the spectrum crunch that affects the most intensively exploited bands. In fact, the RF spectrum shortage is continuously pushing for the opening of higher frequency bands for wireless communications, ranging from millimeter-wave, over terahertz to optical (infrared (IR) or visible) bands [1]–[4]. Each of these possibilities target specific environments and applications, and the ongoing research points towards a combination of access strategies to meet the ever-increasing Internet of Things (IoT) requirements and the associated demand for resources.

In any case, using a specific frequency band for an IoT application is only a part of a wider context. Specifically, in a wireless IoT framework, where the communication medium is

shared, granting a fair access to the shared resources and guaranteeing the link quality in presence of possible interference is of paramount importance [5], [6], while the sporadic nature of the IoT traffic and the short lengths of the exchanged data packets pose specific challenges in this regard. In this context, well designed random access (RA) protocols are instrumental to obtain a good performance of the access network [7]–[12]. Along the last decades, there has been a general trend to embrace interference in wireless media in order to efficiently exploit the available, scarce spectrum resources (e.g. by using spread spectrum or MIMO spatial multiplexing techniques). In the domain of access schemes, the same principle is applied through exploitation of the capture effect, which frequently occurs in wireless communications and through which user data may be recovered in presence of concurrent transmissions. Under such scenarios, collision avoidance ceases to be one the basic design principles for successful RA protocols, because, in fact, promoting collisions may become beneficial. In this way, a simple slotted ALOHA (SA) solution in combination with the exploitation of the capture effect at the physical layer can achieve a favorable throughput performance [13]–[15].

The IoT deployment scenario considered in this paper assumes an indoor space comprising large and unobstructed areas (e.g., a warehouse or an open-plan office), where a large quantity of devices collect, process and send data to a number of access points. In such situation, the use of RF links could lead to an intolerable level of interference and a high probability of packet loss due to collisions. However, transmission technologies based on OWC can help to tackle these challenges, despite their limited coverage. In fact, by resorting to OWC links, the interference across walls is eliminated, and a small scale indoor cellular network could be designed to cover the whole space with a minimal coverage overlapping, thus maximizing the overall throughput.

OWC systems were studied in the recent literature as a potential indoor IoT solution in current and upcoming generations of mobile communication technologies [16]–[23]. For the interested reader, a detailed state-of-the-art of the OWC for the IoT has been presented in [24], mostly focusing on four main IoT domains: Internet of Terrestrial Things (IoTT), Internet of underWater Things (IoWT), Internet of Biomedical Things (IoBT), and Internet of underGround Things (IoGT). Different uplink RA approaches with sporadic and varying device activity in OWC-based IoT systems were analyzed in [25]–[28]. Specifically, [25] analyzed the uplink multi-receiver OWC system in the context of a massive IoT application, where a coded SA approach with successive interference cancellation

This paper was presented in part at the 17th International Symposium On Wireless Communication Systems (ISWCS) 2021 [30].

T. Devaja, M. Petkovic and D. Vukobratovic are with University of Novi Sad, Faculty of Technical Sciences, 21000 Novi Sad, Serbia (e-mails: tijana.devaja@uns.ac.rs; milica.petkovic@uns.ac.rs; dejanv@uns.ac.rs).

F. J. Escribano is with Universidad de Alcalá, Alcalá de Henares, Spain (e-mail: francisco.escribano@uah.es).

Č. Stefanović is with Aalborg University, Aalborg, Denmark (e-mail: cs@es.aau.dk).

was adopted. In [26], Zhao *et al.* analyzed a Multi-Packet Reception (MPR)-aided Visible Light Communications (VLC) system and introduced a novel Quality of Service (QoS)-driven non-carrier sensing RA scheme. The same authors also proposed a novel SA algorithm with heterogeneous delay that guarantees the QoS in the context of the MPR VLC system [27]. An optical camera communication based on the ALOHA RA scheme was assessed in [28], where the access probability of each terminal was optimized in order to guarantee access fairness and system throughput rate maximization.

In this paper, we push the state-of-the-art by analyzing and optimizing a slotted ALOHA-based access scheme that takes into account an advanced modelling of the physical layer via (i) characterization of the signal-to-interference ratio (SINR) in the presence of interfering, randomly activated users and (ii) characterization of the impact of the finite-block length (FBL) effects. The obtained analytical framework allows the derivation of the probability that a user transmission is decoded in the presence of the rest of interfering users. Moreover, other performance metrics can be derived and the access scheme optimized. To the best of our knowledge, this is the first work that investigates the FBL effects in such an OWC environment. In particular, information theory has traditionally focused on data transmission reliability through noisy channels that may be achievable for channel coded data with large block lengths, but the fact is that, for IoT applications, we are usually dealing with short block-length transmissions. In this sense, the so-called FBL information theory [29] provides us with the appropriate tools to analyze what relates to error probability estimation and the corresponding maximum achievable rate under a given message length constraint.

The presented work is an extension of the initial study of the SINR statistics for an OWC-based IoT system with capture effect presented in [30]. In this respect, the main novelty of the paper is the error probability analysis based on FBL theory, as well as the analysis of the overall system throughput and the reliability in terms of the outage probability. The FBL performance analysis for this kind of OWC-based IoT system represents the appropriate method to set the system parameters during the system design, with the aim to achieve an optimal performance of the RA protocol.

The contributions of the paper can be summarized as follows:

1) We propose an architecture for future IoT based on short-range OWC technology and design an access scheme for an OWC-based IoT indoor network. We analyze the scheme in the terms of SINR of the accessing users and evaluate its performance. The analysis builds up on our previous work [30], which is here complemented by the error and coding rate characterization, enabling an accurate modelling of the physical layer effects.

2) The error and the coding rate characterizations are based on the FBL performance analysis for OWC-based IoT systems that is exposed in the paper. Specifically, from SINR statistics it is possible to derive the error probability affecting the captured data packets, protected by an appropriate channel code, thereby determining the system performance.

3) Building up on the physical layer characterization, the

paper presents the analysis of the overall system throughput and the reliability in terms of the outage probability.

4) We use numerical results to provide guidelines for the optimal system design, by exploring the effects of OWC parameters on the system performance. These contributions are particularly important, as a real-world IoT network deployment requires not only that its physical parameters are appropriately set, but also that the access protocol is properly configured to achieve the optimal performance.

The rest of the paper is structured as follows. In Section II, we review the system model and set the main hypothesis. In Section III, we derive the SINR statistics for the proposed setup. In Section IV, we analyze the error probability and channel coding rate based on the FBL regime approach, as well as the overall system throughput and the reliability in terms of the outage probability. In Section V, we present and discuss the numerical results and, finally, in Section VI, we close the paper with the main conclusions.

II. SA-BASED INDOOR OWC IoT: SYSTEM MODEL

The context of this work comprises a communication scenario in which a total of U IoT devices equipped with OWC transmitters contend to access a common OWC access point (AP). The transmitting devices are uniformly placed on a horizontal plane, while the OWC AP is located at the ceiling, at a fixed location (see Fig. 1). This setup corresponds to an open-plan office space with IoT devices placed on tables or other furniture. The SA protocol [9] is used for uplink transmissions. Each IoT device is active for transmission with probability p_a in every slot, independently of its activity in other slots and of the activity of other devices during the same slot period. In other words, we consider Bernoulli arrivals on user basis. If a user is active in a slot, it transmits a fixed-length packet with finite (short) block-length. We denote the set of active users in a slot by \mathcal{U}_a , and by $U_a = |\mathcal{U}_a|$ the corresponding number of active users, where $0 \leq U_a \leq U$. It is straightforward to show that U_a is a random, binomially distributed parameter $\mathcal{B}(U, p_a)$. Finally, with a slight misuse of notation, we denote the individual active users by $u_i \in \mathcal{U}_a$, $i = 1, \dots, U_a$, where their indexing is assigned arbitrarily.

The IoT devices use IR LED sources, and the physical transmission employs a simple intensity-modulation (IM)

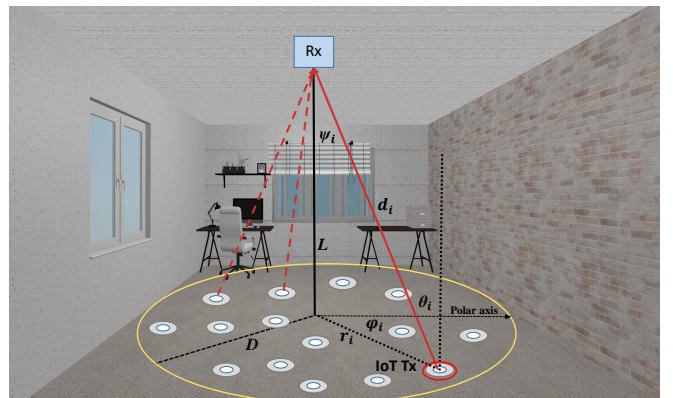


Fig. 1. OWC-based indoor IoT system model.

binary-format signaling (e.g., non-return-to-zero on-off keying, OOK). All devices transmit with the same optical power regardless of any other condition. The OWC photo-detector (PD) receiver performs direct detection (DD) of the arriving light intensity [2]. At any given slot, the light intensity impinging the OWC PD receiver comprises the contribution of the U_a active users plus the background radiation noise. Assuming that the PD is working in a linear regime (which is a standard and a reasonable approximation in practical situations), the received signal after the conversion to the electrical domain (prior to demodulation and decoding) can be modeled as

$$y(t) = \sum_{i=1}^{U_a} P_t \eta h_i x_i(t) + n(t), \quad (1)$$

where $x_i(t)$, $i = 1, \dots, U_a$, is the unit-power signal waveform of the active user u_i , P_t is the transmitted optical power, η the optical-to-electrical conversion coefficient, $h_i \geq 0$ the optical channel gain from the user u_i to the AP, while $n(t)$ is an instance of additive white Gaussian noise with power spectral density $N_0/2$. This kind of noise process adequately models the distorting effects of the optical background radiation and the receiver thermal noise, and contributes to the overall signal-to-noise with a noise power $\sigma_n^2 = N_0 B$, where B is the system noise bandwidth.

Under these conditions, if a slot contains transmissions from two or more users (i.e., $U_a \geq 2$ for such slot), a packet collision takes place. In that case, by exploiting the capture effect, the OWC AP receiver will try to decode the colliding transmissions, in contrast to the classical SA scheme, which assumes the collision channel model. We are interested in the probability that the receiver succeeds in decoding a randomly selected user among the set of active ones. For convenience, and without loss of generality, we assume that the index of such user (denoted as the *reference user* henceforth) corresponds to $i = 1$, i.e., u_1 is the reference user, while the rest of the active users u_i , $i = 2, \dots, U_a$, are the interfering ones. Therefore, the received signal (1) can be rewritten as

$$y(t) = P_t \eta h_1 x_1(t) + \sum_{i=2}^{U_a} P_t \eta h_i x_i(t) + n(t), \quad (2)$$

where $x_1(t)$ is the signal waveform from the reference user u_1 , $h_1 \geq 0$ is the corresponding optical channel gain, and the summation term represents the interference contribution from all other active users.

Based on (2), the SINR experienced by the reference user can be readily written as

$$\text{SINR} = \frac{P_t \eta^2 h_1^2}{\sum_{i=2}^{U_a} P_t \eta^2 h_i^2 + \sigma_n^2} = \frac{\gamma_1}{\sum_{i=2}^{U_a} \gamma_i + 1} = \frac{\gamma_1}{\gamma_1 + 1}, \quad (3)$$

where

$$\gamma_1 = \frac{P_t \eta^2 h_1^2}{\sigma_n^2}, \quad \gamma_i = \frac{P_t \eta^2 h_i^2}{\sigma_n^2}, \quad \gamma_i = \sum_{i=2}^{U_a} \gamma_i. \quad (4)$$

The SINR depends not only on the number of active users, but also on the specific placements of the IoT devices with respect to the OWC AP (which, in turn, determines the specific values

of the optical path gains, h_i). In the next section, we derive the statistics for the SINR observed by a randomly selected active user, based on the characteristics of the system setup and its optical parameters.

III. SINR STATISTICS FOR THE SA-BASED OWC IoT SYSTEM

As shown in Fig. 1, we assume that the devices are randomly and uniformly distributed over the same horizontal plane within the indoor circular coverage area of radius D . The OWC AP is positioned at a height L above the plane, over the center of the circle. The location of user u_i with respect to the OWC AP is determined by the angle θ_i (angle of irradiance), the angle φ_i , and the radius r_i in the polar coordinate plane. Furthermore, the corresponding angle of incidence into the AP is denoted as ψ_i , and the Euclidean distance between the corresponding LED transmitter and the PD receiver is denoted as d_i . The optical channel gain of the line-of-sight (LoS) link between u_i and the PD receiver can be determined as [31]

$$h_i = \frac{A_r (m+1) R_r}{2\pi d_i^2} \cos^m(\theta_i) T_s g(\psi_i) \cos(\psi_i), \quad (5)$$

where A_r is the surface area of the PD, R_r is the responsivity, T_s is the gain of the optical filter, $g(\psi_i)$ is the response of the optical concentrator, and the factor m is described in the sequel. The optical concentrator is modeled as $g(\psi_i) = \zeta^2 / \sin^2(\Psi)$, for $0 \leq \psi_i \leq \Psi$, where ζ is the refractive index of the lens at the PD and Ψ denotes its field of view (FoV). Finally, the LED emission follows a generalized Lambertian radiation pattern with order $m = -\ln 2 / \ln(\cos \Phi_{1/2})$, where $\Phi_{1/2}$ denotes the semi-angle at half illuminance¹ [2].

In this situation, if the surface of the PD receiver is parallel to the plane where the IoT devices are located, then $\theta_i = \psi_i$, $d_i = \sqrt{r_i^2 + L^2}$, $\cos(\theta_i) = \frac{L}{\sqrt{r_i^2 + L^2}}$, and equation (5) can be rewritten as

$$h_i = \frac{\mathcal{X}}{(r_i^2 + L^2)^{\frac{m+3}{2}}}, \quad (6)$$

where $\mathcal{X} = \frac{A_r(m+1)R_r}{2\pi} T_s g(\psi_i) L^{m+1}$ is a factor that does not depend on the specific placement of the IoT device, provided that the angle ψ_i lies below the PD FoV (a condition met for the values of D and L considered here, so that there would be no IoT devices excluded from the coverage area of the AP).

As the IoT devices are uniformly distributed, the PDF of their radial distance r_i from the centre of the circle is [32]

$$f_{r_i}(r) = \frac{2r}{D^2}, \quad 0 \leq r \leq D. \quad (7)$$

By using expressions (6) and (7), and standard RV transformation techniques, the PDF of the optical channel gains, h_i , can be derived as

$$f_{h_i}(h) = \frac{2\mathcal{X}^{\frac{2}{m+3}}}{D^2(m+3)} h^{-\frac{m+5}{m+3}}, \quad h_{\min} \leq h \leq h_{\max}, \quad (8)$$

where $h_{\min} = \frac{\mathcal{X}}{(D^2 + L^2)^{\frac{m+3}{2}}}$ and $h_{\max} = \frac{\mathcal{X}}{L^{m+3}}$.

¹We assume that all LEDs are characterized by the same parameters, i.e., $m_i = m$ and $\Phi_{1/2}^i = \Phi_{1/2} \forall i$.

The PDF of γ_i , defined in (4), can be similarly derived as [32]

$$f_{\gamma_i}(\gamma) = \frac{(\mu\mathcal{X}^2)^{\frac{1}{m+3}}}{D^2(m+3)} \gamma^{-\frac{m+4}{m+3}}, \quad \gamma_{\min} \leq \gamma \leq \gamma_{\max}, \quad (9)$$

where $\gamma_{\min} = \frac{\mu\mathcal{X}^2}{(D^2+L^2)^{m+3}}$, $\gamma_{\max} = \frac{\mu\mathcal{X}^2}{L^{2(m+3)}}$, and $\mu = \frac{P_t \eta^2}{\sigma_n^2}$.

The CDF of γ_i can be easily derived as

$$F_{\gamma_i}(\gamma) = \begin{cases} 1 + \frac{L^2 - (\mu\mathcal{X}^2/\gamma)^{\frac{1}{m+3}}}{R^2}, & \gamma_{\min} \leq \gamma \leq \gamma_{\max} \\ 1, & \gamma > \gamma_{\max} \end{cases}. \quad (10)$$

To get the statistical characterization of the overall SINR, we can use the characteristic function (CF) approach [33]. In this case, the CF of $\gamma_i = \frac{P_t \eta^2 h_i^2}{\sigma_n^2}$ can be derived via (9) as

$$\begin{aligned} \varphi_{\gamma_i}(t) &\triangleq \mathbb{E}[e^{jt\gamma_i}] = \int_{\gamma_{\min}}^{\infty} e^{jtx} f_{\gamma_i}(\gamma) d\gamma \\ &= \frac{(\mu\mathcal{X}^2)^{\frac{1}{m+3}}}{D^2(m+3)} \int_{\gamma_{\min}}^{\gamma_{\max}} \gamma^{-\frac{m+4}{m+3}} e^{jtx} d\gamma = \frac{(\mu\mathcal{X}^2)^{\frac{1}{m+3}}}{D^2(m+3)} \\ &\times \left(\Gamma\left(-\frac{1}{m+3}, -jt\gamma_{\min}\right) - \Gamma\left(-\frac{1}{m+3}, -jt\gamma_{\max}\right) \right), \end{aligned} \quad (11)$$

where $\Gamma(s, z) = \int_z^{\infty} t^{s-1} e^{-t} dt$ is the upper incomplete gamma function [34, (8.35)].

A. Contribution to the SINR Statistics from the Reference User

For the reference user, the PDF of γ_1 can be calculated as a particular case of equation (9), rewritten here for clarity

$$f_{\gamma_1}(\gamma) = \frac{(\mu\mathcal{X}^2)^{\frac{1}{m+3}}}{D^2(m+3)} \gamma^{-\frac{m+4}{m+3}}, \quad \gamma_{\min} \leq \gamma \leq \gamma_{\max}. \quad (12)$$

B. Contribution to the SINR Statistics from the Interfering Users

The channel gains h_i (thus also γ_i) are independent and identically distributed (i.i.d.) RVs when the IoT device locations are also i.i.d. RVs. In this case, the CF of $\gamma_1 = \sum_{i=2}^{U_a} \gamma_i$ can be determined as [33]

$$\begin{aligned} \varphi_{\gamma_1}(t) &\triangleq \mathbb{E}[e^{jt\gamma_1}] = \mathbb{E}\left[e^{jt \sum_{i=2}^{U_a} \gamma_i}\right] = \mathbb{E}\left[\prod_{i=2}^{U_a} e^{jt\gamma_i}\right] \\ &= \prod_{i=2}^{U_a} \mathbb{E}[e^{jt\gamma_i}] = \prod_{i=2}^{U_a} \varphi_{\gamma_i}(t) = \varphi_{\gamma_i}^{U_a-1}(t), \end{aligned} \quad (13)$$

where the CF of γ_i is defined in (11). The PDF of γ_1 can be derived as

$$\begin{aligned} f_{\gamma_1}(\gamma) &= \frac{1}{2\pi} \int_{-\infty}^{\infty} e^{-jtx} \varphi_{\gamma_1}(t) dt \\ &= \frac{1}{2\pi} \int_{-\infty}^{\infty} e^{-jtx} \varphi_{\gamma_i}^{U_a-1}(t) dt, \end{aligned} \quad (14)$$

for $\gamma_{\min}^{U_a-1} \leq \gamma \leq \gamma_{\max}^{U_a-1}$.

C. Overall SINR Statistics for the Reference User

As an intermediate step, we derive the PDF of the RV defined as $\lambda = \gamma_1 + 1$, namely

$$\begin{aligned} f_{\lambda}(\lambda) &= \frac{f_{\gamma_1}(\gamma_1)}{\left|\frac{d\lambda}{d\gamma_1}\right|} = f_{\gamma_1}(\lambda - 1) \\ &= \frac{1}{2\pi} \int_{-\infty}^{\infty} e^{-jt(\lambda-1)} \varphi_{\gamma_i}^{U_a-1}(t) dt, \end{aligned} \quad (15)$$

for $\gamma_{\min}^{U_a-1} + 1 \leq \lambda \leq \gamma_{\max}^{U_a-1} + 1$. Since γ_1 and γ_1 are independent RVs, their joint PDF is $f_{\gamma_1, \lambda}(x, \lambda) = f_{\gamma_1}(x) f_{\lambda}(\lambda)$. The PDF of the SINR $= \frac{\gamma_1}{\lambda} = \frac{\gamma_1}{\gamma_1 + 1}$ of the reference user, conditioned on the total number of active users U_a , can be written as follows [35]

$$f_{\text{SINR}}(x|U_a) = \int_{-\infty}^{\infty} |\lambda| f_{\gamma_1}(x\lambda) f_{\lambda}(\lambda) d\lambda, \quad (16)$$

where $f_{\gamma_1}(x)$ and $f_{\lambda}(\lambda)$ are defined in equations (12) and (15), respectively. After replacing (12) and (15) in equation (16), since $\lambda > 0$, this PDF can be written as

$$\begin{aligned} f_{\text{SINR}}(x|U_a) &= \frac{(\mu\mathcal{X}^2)^{\frac{1}{m+3}}}{2\pi D^2(m+3)} x^{-\frac{m+4}{m+3}} \\ &\times \int_{\gamma_{\min}^{U_a-1}+1}^{\gamma_{\max}^{U_a-1}+1} \lambda^{-\frac{1}{m+3}} \left(\int_{-\infty}^{\infty} e^{-jt(\lambda-1)} \varphi_{\gamma_i}^{U_a-1}(t) dt \right) d\lambda, \end{aligned} \quad (17)$$

where $\varphi_{\gamma_i}(t)$ is the CF previously defined in equation (11).

Finally, the CDF of the SINR of the reference user, conditioned on the number of active users in the slot U_a , can be written as

$$F_{\text{SINR}}(\gamma|U_a) = \int_0^{\gamma} f_{\text{SINR}}(x|U_a) dx. \quad (18)$$

This statistical characterization of the SINR will allow us to derive the error probability in the next section.

IV. PERFORMANCE ANALYSIS FOR THE OWC-BASED IoT SYSTEM BASED ON SA VIA THE FBL APPROACH

A. Error Probability for SA via the FBL approach

The basic goal of information theory is to quantify the extent to which reliable communication is possible over a noisy channel. A code of size N and block length n allows the communication of one of N messages via n uses of the channel. The fundamental trade-off between these quantities and the reliability of the communication process is captured by $N_{\epsilon}(n)$ – the largest size of the code with error probability ϵ (assuming equiprobable messages). A related, commonly used metric is the code rate $R = \log_2 N/n$. In this respect, investigating which is the maximum code rate $R_{\epsilon}(n)$ that allows a communication with n channel uses while providing reliability ϵ is the central question of FBL theory.

Building upon the classical Shannon's asymptotic results, Polyanskiy, Poor, and Verdu showed that for the additive white Gaussian noise (AWGN) channel with capacity $C(\gamma) = \log_2(1 + \gamma)$, where γ denotes the signal-to-noise ratio (SNR), the maximal achievable rate with decoding error probability ϵ can be tightly approximated as [29]

$$R = C(\gamma) - \sqrt{\frac{V_{\text{AWGN}}(\gamma)}{n}} Q^{-1}(\epsilon) + O\left(\frac{\log n}{n}\right), \quad (19)$$

where $Q^{-1}(\cdot)$ denotes the inverse of the Gaussian Q-function defined as $Q(z) = \int_z^\infty \frac{1}{\sqrt{2\pi}} e^{-\frac{t^2}{2}} dt$, while the so-called channel dispersion $V_{\text{AWGN}}(\gamma)$ is defined as

$$V_{\text{AWGN}}(\gamma) = \left(1 - \frac{1}{1 + \gamma^2}\right) \log_2^2(e). \quad (20)$$

In the context of this work, we are interested in the error probability of decoding a short-length data packet from a single active user by taking into account the interference contribution from all other active users in a given slot, see (3). Using the standard “treat interference as noise” approximation, one may initially consider the interference as an additional and independent Gaussian noise process. Strictly speaking, however, the aggregate interference does not obey Gaussian statistics (to achieve (19), transmitters need to use a non-Gaussian codebook), implying that the OWC receiver experiences non-Gaussian interference. A more precise and appropriate approximation is provided in [36], where non-Gaussian interference and nearest-neighbor decoding are assumed. In this case, the channel dispersion derived in [36] (see also [37]) should be applied, i.e.,

$$V(\gamma) = \frac{2\gamma}{1 + \gamma} \log_2^2(e), \quad (21)$$

instead of (20). On the other hand, for $n > 100$ channel uses, the term $O(\frac{\log n}{n})$ in (19) becomes negligible and can be omitted. Taking all this into account, the achievable rate could be tightly approximated as

$$R \approx C(\gamma) - \sqrt{\frac{V(\gamma)}{n}} Q^{-1}(\epsilon). \quad (22)$$

It is to be noted that the approximation (22) is established by characterizing the asymptotic behavior of analytically tractable achievability and converse bounds (see [29, Sec. III]).

For the system setup considered in this paper, relying on equation (22) and by setting $\text{SINR} = \gamma$ (which is dependent on the number of active users U_a), we can tightly approximate the decoding error probability as

$$\epsilon(\gamma, U_a) = Q\left(\sqrt{\frac{n}{V(\gamma(U_a))}} (C(\gamma(U_a)) - R)\right). \quad (23)$$

For the sake of clarity, in the previous equation we make the dependence of the error probability $\epsilon(\gamma, U_a)$ on the number of active users U_a explicit, although this dependence is implicit through the dependence of the SINR statistics $\gamma(U_a)$ on the number of active users U_a . By conditioning the error probability over the SINR, we get

$$\epsilon(U_a) = \int_{\gamma} \epsilon(\gamma, U_a) f_{\text{SINR}}(\gamma|U_a) d\gamma, \quad (24)$$

where $f_{\text{SINR}}(\gamma|U_a)$ was previously derived in (17). Finally, the unconditional error probability can be derived as

$$\epsilon = \sum_{k=1}^U \epsilon(U_a = k) \mathbb{P}[U_a = k], \quad (25)$$

where

$$\mathbb{P}[U_a = k] = \binom{U}{k} p_a^k (1 - p_a)^{U-k}, \quad k = 0, \dots, U, \quad (26)$$

i.e., the number of active users U_a is a binomial random variable for the assumed Bernoulli arrival process.

B. Throughput for SA via the FBL approach

The overall system throughput is analysed as the parameter that describes the effective information transmission rate in the system. Based on the system throughput performance, it can be determined if channel uses are effectively exploited, not only due to the effects of the noise but also due to the interference among randomly activated users.

Considering the FBL regime with the fixed code rate R , and the probability that the packet is decoded at each slot as derived previously in (25), we define the throughput as

$$\begin{aligned} T &= 0 \cdot \mathbb{P}[U_a = 0] + \sum_{k=1}^U R \cdot (1 - \epsilon(U_a = k)) \cdot \mathbb{P}[U_a = k] \\ &= R \cdot (\mathbb{P}[U_a > 0] - \epsilon) \\ &= R \cdot ((1 - (1 - p_a)^U) - \epsilon), \end{aligned} \quad (27)$$

where $\mathbb{P}[U_a > 0] = 1 - (1 - p_a)^U$ represents the probability that at least one user is active during the slot.

C. Outage Probability for SA via the FBL approach

We also analyze the system reliability in terms of the outage probability of a single transmission. We consider that the outage will happen if the overall SINR falls below a predetermined SINR threshold, denoted by γ_{th} .

For the system under consideration, and under the FBL regime with the selected code rate R , a predetermined γ_{th} threshold can be defined as a minimal value of the received SINR required to achieve a certain value of the error probability ϵ_{th} . Based on (23), the outage threshold can be determined as

$$\gamma_{\text{th}} = \Phi^{-1}(\epsilon_{\text{th}}), \quad (28)$$

where $\gamma = \Phi^{-1}(\epsilon)$ is obtained by inverting the expression in equation (23).

Considering the transmission from the reference user, the outage probability can be determined as

$$P_{\text{out}}(U_a) = \mathbb{P}[\text{SINR} < \gamma_{\text{th}} | U_a] = F_{\text{SINR}}(\gamma_{\text{th}} | U_a), \quad (29)$$

where $F_{\text{SINR}}(\gamma_{\text{th}} | U_a)$ is in (18). The unconditional outage probability can be calculated as

$$P_{\text{out}} = \sum_{k=1}^U P_{\text{out}}(U_a = k) \mathbb{P}[U_a = k], \quad (30)$$

where $\mathbb{P}[U_a = k]$ was calculated in (26). Note that the reliability can be simply calculated as $P_R = 1 - P_{\text{out}}$.

D. Special Case: SA without Capture in the FBL Regime

The classical SA scheme without capture effect assumes that if more than one user is active in a given slot, a collision will happen and the packet is lost. Contrary to SA with capture, the classical SA receiver will only recover the packet if just

one of the U IoT devices is active, i.e., $U_a = 1$. In that case, $\epsilon(U_a = k) = 0$ for $k > 1$, and thus the error probability is

$$\epsilon = \epsilon(U_a = 1) \mathbb{P}[U_a = 1], \quad (31)$$

where $\epsilon(U_a = 1)$ and $\mathbb{P}[U_a = 1]$ are determined by expressions (25) and (26), respectively, where $k = 1$.

Based on this, the throughput for SA without capture via the FBL approach can be defined as

$$\begin{aligned} T &= 0 \cdot \mathbb{P}[U_a = 0] + R \cdot (1 - \epsilon(U_a = 1)) \cdot \mathbb{P}[U_a = 1] \\ &+ \sum_{k=2}^U R \cdot (1 - \epsilon(U_a = k)) \cdot \mathbb{P}[U_a = k] \\ &= R \cdot (\mathbb{P}[U_a = 1] - \epsilon) \end{aligned} \quad (32)$$

since $\epsilon(U_a = k) = 0$ for $k > 1$.

The outage probability for the OWC system based on SA without capture in the FBL regime can be calculated as

$$P_{\text{out}} = P_{\text{out}}(U_a = 1) \mathbb{P}[U_a = 1] \quad (33)$$

since $P_{\text{out}}(U_a = k) = 0$ for $k > 1$.

Note that there will be no interference contribution under this scenario, since packet can be decoded only if one user is active. According to this, for the error probability derivation in (24), the PDF given by (9) will be considered instead of the PDF $f_{\text{SINR}}(\gamma|U_a)$ derived in (17). Similarly, the outage probability will be derived based in the CDF given by (10) instead of the CDF of the SINR $F_{\text{SINR}}(\gamma|U_a)$ derived in (18).

V. NUMERICAL RESULTS AND DISCUSSION

In this section, using the analysis presented in Sec. III and Sec. IV, we focus on the design and performance evaluation of the proposed indoor OWC IoT system. The results are obtained by adopting the system parameters given in Table I, which represent a typical situation in such environment. Further, since both the PDF and CDF of the SINR in (17) and (18), respectively, are given in integral form, the results are obtained by numerical computations performed through the FFT algorithm implemented in MATLAB.

Fig. 2 presents the CDF of the SINR derived in (18), comparing the results obtained by the numerical computations with the ones obtained via Monte Carlo (MC) simulations. Obviously, these results match each other, validating the analysis performed in the previous section. In addition, we note that an increase in U_a leads to a situation in which the SINR progressively degrades, which could be expected.

TABLE I
System parameters

name	symbol	value
Transmitted optical power	P_t	30 mW
Photodetector surface area	A_r	1 cm ²
Responsivity	R_r	0.4 A/W
Optical filter gain	T_s	1
Refractive index of lens at a PD	ζ	1.5
FoV of receiver	Ψ	90°
Optical-to-electrical conversion efficiency	η	0.8
Noise power spectral density	N_0	10 ⁻²¹ W/Hz
System noise bandwidth	B	$B = 200$ kHz

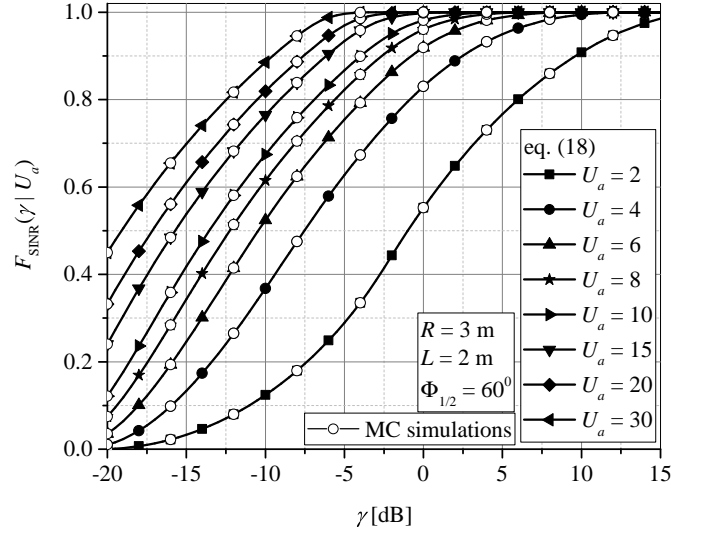


Fig. 2. SINR CDF of the reference user conditioned on U_a , $F_{\text{SINR}}(\gamma_{\text{th}}|U_a)$.

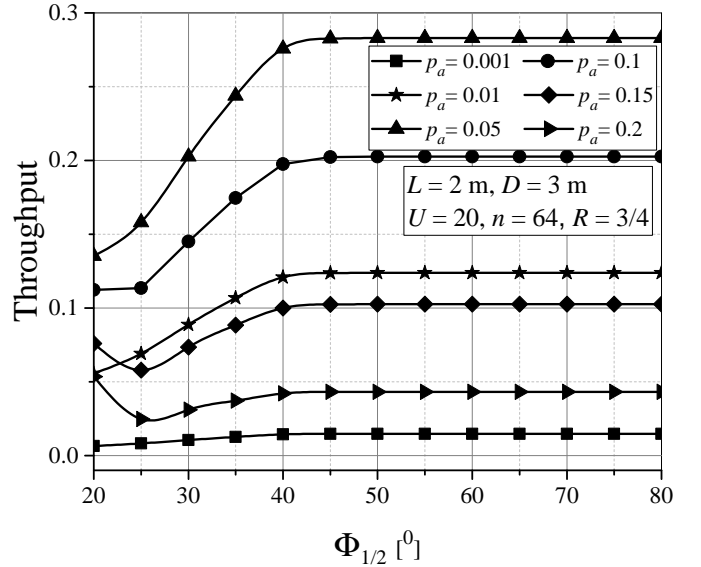


Fig. 3. Throughput vs. $\Phi_{1/2}$ for different activation probability values p_a .

Fig. 3 depicts the dependence of the throughput on the semi-angle at half illuminance $\Phi_{1/2}$, evaluated using the expression derived in (27), and considering different values of the activation probability p_a . An increase in p_a up to a certain value results in a better performing system from the throughput point of view. However, after this value of p_a is surpassed, the throughput starts to decrease. In fact, it can be seen that there is an optimal value of p_a that maximizes the throughput performance of the system. On the other hand, depending on p_a (i.e., the number of active OWC-based IoT devices), a higher value of $\Phi_{1/2}$ may improve or degrade the system performance. The semi-angle at half illuminance of the LED determines the Lambertian order of the LED source, or, in other words, determines the received optical signal intensity from the active IoT users at the OWC AP. When the value of $\Phi_{1/2}$ is higher, the optical beam at the LED source output

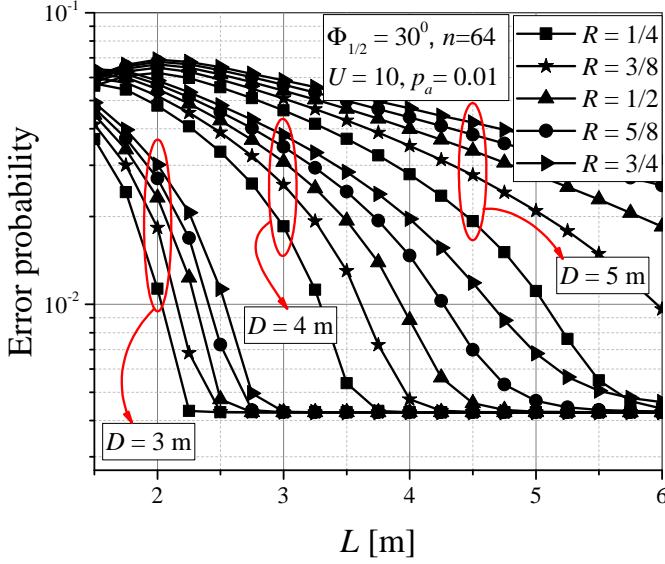


Fig. 4. Error probability vs. L for different values of the rate R and the radius D .

will be wider, thus the received power from the users that are not close from the AP will be higher. This holds for all IoT devices, thus the semi-angle will have a strong impact on both the reference user and the interference contributions (i.e., on the overall received SINR). To conclude, since $\Phi_{1/2}$ represents an important parameter which has a substantial impact on the received optical signal intensity, the number of active users (together with the overall interference) will determine if an increase in $\Phi_{1/2}$ leads to a higher or a lower system throughput.

Fig. 4 depicts the error probability of the considered OWC system in the FBL regime, as derived in (25), as a function of the OWC AP height L , for various levels of error protection parameterized by the code rate R . Additionally, three different values of radius D are considered. As expected, increasing R will result in an error protection performance deterioration. When the radius D is larger, the OWC IoT users will be distributed over a wider area, which will increase the chance that many of them are far distant from the OWC AP. Increasing the distance of the OWC users from the AP leads to a reduced received power, and consequently the overall SINR will be lower. This will affect the capture probability, and thus the error probability of the system will increase when D increases. Further, Fig. 4 shows that there is an error probability floor, which is reached for lower values of L as the radius D gets smaller. When the users are located in a wider area, the error floor appears at very high L . Note that the error probability floor is independent on the code rate R , as well as on the radius D . In other words, increasing the distance between the planes where the IoT users and the OWC AP are placed will not result in lower-error probability after the error floor is reached, for any value of D and R . Consequently, the geometric setup of the OWC based IoT framework has an impact on the system performance behavior in the FBL regime.

Fig. 5 presents the error probability ϵ of the considered OWC system under the FBL regime, derived in (25), as a

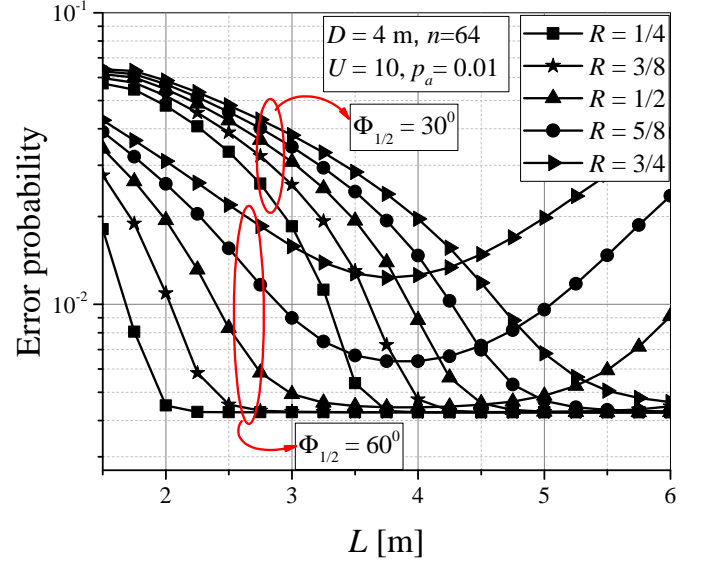


Fig. 5. Error probability vs. L for different values of the rate R and the semi-angle $\Phi_{1/2}$.

function the OWC AP height L , for different code rates R . In contrast to Fig. 4, the system behavior here is observed for two different values of the semi-angle at half illuminance $\Phi_{1/2}$. Similarly to Fig. 3, the system behaves differently when the value of $\Phi_{1/2}$ increases. For example, when $L < 3$ m, the error probability is lower for the larger semi-angle $\Phi_{1/2}$ value, whereas for $L > 5$ m, the system performance degrades sharply for higher values of $\Phi_{1/2}$. Additionally, a larger distance from the OWC IoT users to the AP (i.e., greater L) leads to a reduced received power, and to a lower overall SINR. This will affect the capture probability in such a way that larger L results in a behavior where the error probability of the system considered will initially decrease (eventually reaching the error probability floor in some cases), and, after some point that is dependent on $\Phi_{1/2}$, it will increase. Moreover, there is a minimum value of the error rate for different OWC system setups, determined by the semi-angle $\Phi_{1/2}$ and the overall distance from the OWC IoT users to the AP. From Figs. 4 and 5, it can be concluded that the effects of the rate value on the error probability performance is mainly dependent on the parameters L and $\Phi_{1/2}$.

Fig. 6 shows the dependence of the throughput derived in (27) on the activation probability p_a for different number of OWC-based IoT devices U and different values of radius D . As previously stated, a higher value of the radius D leads to a worse system performance, i.e., to a lower throughput level. A higher activation probability p_a and a higher number of total users U implies a higher number of active users in a slot. The number of active IoT devices determines the overall SINR, which has a direct impact on the potential of the capture effect. Consequently, as for the trend of each curve, it can be seen how, when the total number of users U in the system gets higher, the optimal value of p_a that maximizes T gets lower. Moreover, after achieving its maximum value, the system throughput starts decreasing with a further increase of

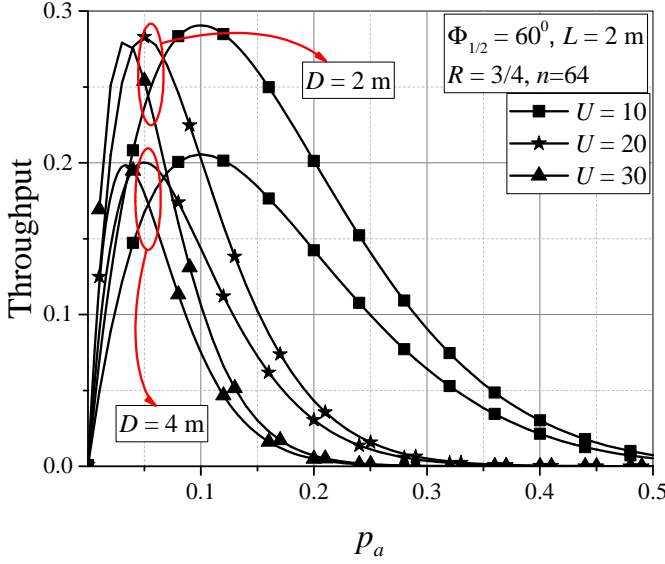


Fig. 6. Throughput vs. p_a for different number of total IoT devices U .

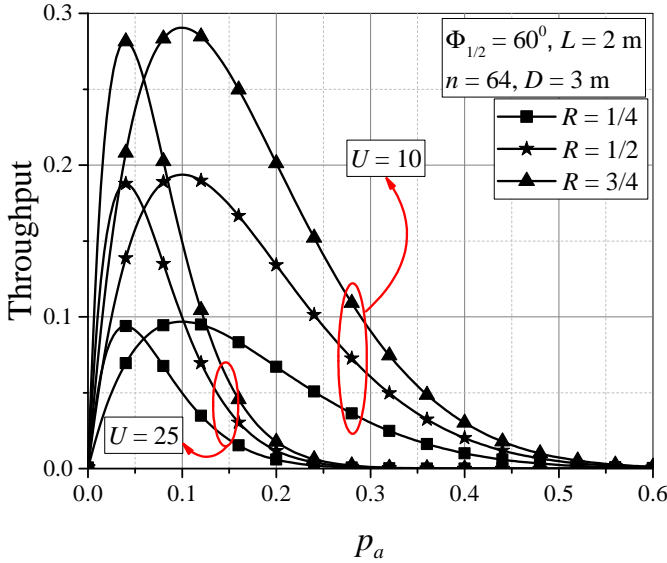


Fig. 7. Throughput vs. p_a for different values of the maximum achievable rate R .

p_a . Given the radius D , the maximum value of the throughput is rather insensitive to the number of users. On the other hand, the optimal value of p_a that maximizes the throughput depends on the total number of users U , but, given U it remains the same irrespective to the change in D . In conclusion, we can say that the geometric setup of the OWC based IoT system and the total number of users have strong impact on the optimal system performance, and should be taken into consideration during the design of the access protocol.

In Fig. 7, we show the throughput derived in (27) as a function of the activation probability p_a for different values of the maximum achievable rate R . As previously stated, a higher rate corresponds to a degraded system performance. Moreover, Fig. 7 also reveals that there is an optimal value of p_a that leads to a maximum value of the system throughput.

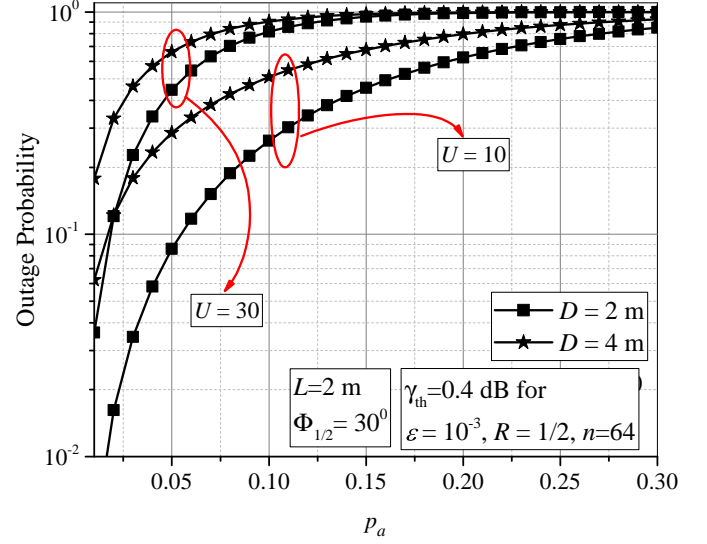


Fig. 8. Outage probability vs. p_a for different values of the radius D and different number of users U .

From the presented results, it can be concluded that the optimal value of p_a differs for different number of overall users, but it is the same regardless of the employed rate R .

Based on the expression derived in (30), Fig. 8 depicts the outage probability dependence on the activation probability p_a , considering two values for the radius D ($D = 2$ m and $D = 4$ m). The outage threshold γ_{th} was defined in (28), and is obtained for an error probability of $\epsilon_{th} = 10^{-3}$, a rate $R = 1/2$ and a number of channel uses $n = 64$. As previously stated, a smaller value of the radius D results in a better system performance. As shown in the figure, a higher number of users lead to a system performance deterioration, since the interference contribution will be stronger. Furthermore, it can be noticed that the radius D and the total number of users U have an effect on the outage performance only for a smaller number of active users, while when $p_a > 0.25$ the radius D and the number U seem to have no impact on the outage probability. More precisely, the system outage will happen for $p_a > 0.3$, i.e., $P_{out} \approx 1$, for any D and U , since the overall SINR will not be higher than γ_{th} and the error probability target value $\epsilon_{th} = 10^{-3}$ will not be achieved.

Figs. 9 and 10 present the overall throughput comparison of the proposed SA OWC IoT system with capture (eq. (27)), and the SA system without capture effect (eq. (32)), in the FBL regime.

Fig. 9 shows the throughput dependence on p_a for various levels of error protection parameterized by the code rate R . A significant improvement of the system throughput is noticed in presence of the capture effect, especially for large code rates R . The results prove that the designed RA protocol represents an improvement from the point of view of the throughput, since user data can be recovered even in presence of concurrent transmissions thanks to the successful exploitation of the capture effect.

Fig. 10 depicts the throughput dependence on p_a for two values of the semi-angle $\Phi_{1/2}$. The throughput improvement

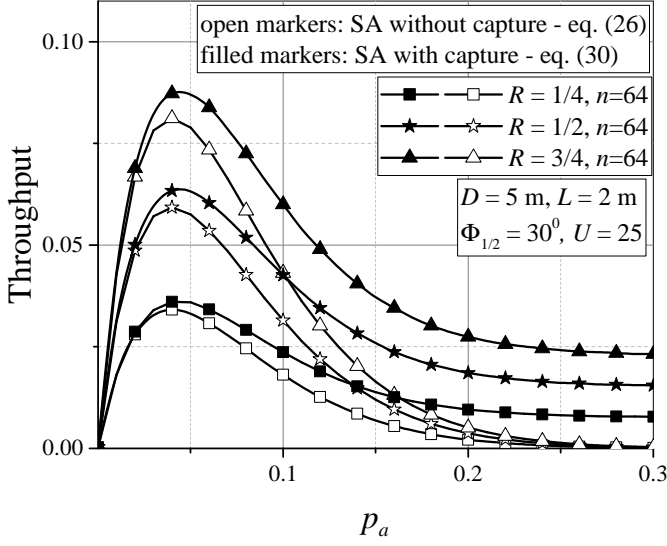


Fig. 9. Comparisons of the throughput of the system with and without capture effect for different values of the rate R .

achieved by employing SA with capture is only evident for the lower semi-angle of $\Phi_{1/2} = 30^\circ$. As a contrast, the throughput remains the same when the semi-angle is higher, i.e., $\Phi_{1/2} = 60^\circ$. It can be concluded that the semi-angle of the OWC system plays a crucial role with respect to the interference contribution and its effects. More specifically, the capture effect leads to significant throughput improvement under the specific condition of limited interference (i.e. lower semi-angle), as may be expected.

In summary, we can conclude that the geometric setup (including the semi-angle at half illuminance $\Phi_{1/2}$, the radius D and the height L), the number of active users, and the code rate R play an important role in the possible maximization of the system performance. These parameters should be taken into account in order to appropriately design an access scheme in an OWC-based IoT system.

VI. CONCLUSION

In this paper, we have analyzed the uplink of an indoor OWC-based IoT system under the FBL regime and with a single access point. The system employs a SA-based access scheme, which exploits the capture effect, i.e., the possibility to decode user transmissions in the presence of interference from other users, which inherently exists in such setups. Based on the received SINR statistics, an analytical expression for the error probability in the FBL regime has been derived, as well as an expression for the overall throughput and the outage probability of the system under investigation. The derived expressions are used to obtain numerical results, which are further analyzed to assess the system performance behavior depending on the OWC framework and the channel model parameters.

The results presented have shown how the geometric setup of the OWC-based IoT system and the activation probability affect the error probability, the throughput and the outage probability performance. It has been proven that the OWC-based system geometry has a significant impact on the overall

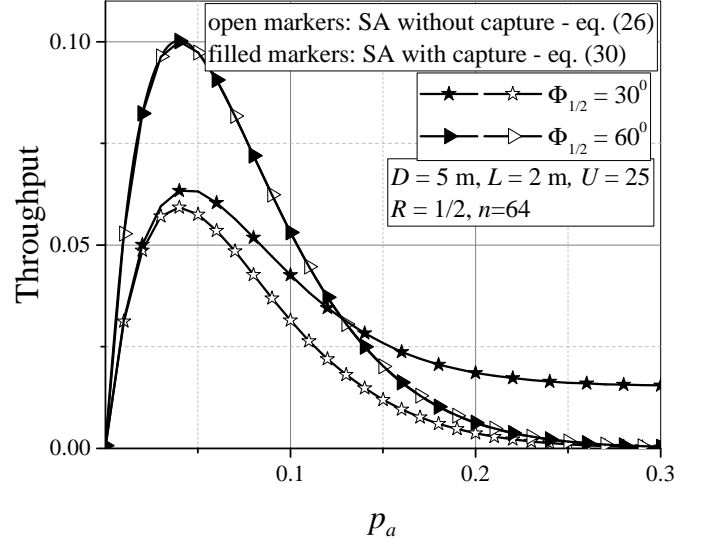


Fig. 10. Comparisons of the throughput of the system with and without capture effect for different values of the semi-angle $\Phi_{1/2}$.

system performance, and should be taken into account during the design of any indoor OWC-based IoT system in order to assess and optimize the RA protocol performance.

ACKNOWLEDGMENT

This work has received funding from the European Union Horizon 2020 research and innovation programme under the grant agreement No 856967 and by the Secretariat for Higher Education and Scientific Research of the Autonomous Province of Vojvodina through the project “Visible light technologies for indoor sensing, localization and communication in smart buildings” (142-451-2686/2021). This research was supported by the Science Fund of the Republic of Serbia, Program DIASPORA, #GRANT 6393139, AVIoTION and by the European Union COST Action CA19111.

REFERENCES

- [1] M. Z. Chowdhury, M. T. Hossan, and Y. M. Jang, “A Comparative Survey of Optical Wireless Technologies: Architectures and Applications,” *IEEE Access*, vol. 6, pp. 9819-9840, 2018.
- [2] Z. Ghassemlooy, W. Popoola, and S. Rajbhandari, *Optical Wireless Communications: System and Channel Modelling With MATLAB®*. Boca Raton, FL, USA: CRC Press, 2013.
- [3] Z. Ghassemlooy, L. N. Alves, S. Zvanovec, and M. A. Khalighi, (Eds.), *Visible Light Communications: Theory and Applications*. Boca Raton, FL, USA: CRC Press, 2017.
- [4] Z. Ghassemlooy, S. Arnon, M. Uysal, Z. Xu, and J. Cheng, “Emerging Optical Wireless Communications-Advances and Challenges,” *IEEE J. Sel. Areas Commun.*, vol. 33, no. 9, pp. 1738-1749, Sept. 2015.
- [5] P. Popovski, *Wireless Connectivity: An Intuitive and Fundamental Guide*. John Wiley & Sons, 2020.
- [6] M. Berlioli, G. Cocco, G. Liva, and A. Munari, *Modern random access protocols*, Foundations and Trends® in Networking, vol. 10, no.4, pp. 317-446, 2016.
- [7] R. Rom and M. Sidi, *Multiple access protocols: performance and analysis*. Springer Science & Business Media, 2012.
- [8] F. Clazzer, A. Munari, G. Liva, F. Lazaro, C. Stefanovic, and P. Popovski, “From 5G to 6G: Has the time for modern random access come?” in *Proc. 1st 6G summit*, Levi, Finland, Mar. 2019.
- [9] L. G. Roberts, “ALOHA packet system with and without slots and capture,” *ACM SIGCOMM Comput. Commun. Review.*, vol. 5, no. 2, pp. 28-42, 1975.

- [10] A. Munari, F. Clazzer, G. Liva, and M. Heindlmaier, "Multiple-relay slotted ALOHA: performance analysis and bounds," *IEEE Trans. Commun.*, vol. 69, no. 3, pp. 1578–1594, 2021.
- [11] W. S. Jeon, S. B. Seo and D. G. Jeong, "POMDP-Based Contention Resolution for Framed Slotted-ALOHA Protocol in Machine-Type Communications," *IEEE Internet of Things J.*, vol. 9, no. 15, pp. 13511–13523, Aug. 2022.
- [12] J. F. Grybosi, J. L. Rebelatto and G. L. Moritz, "Age of Information of SIC-Aided Massive IoT Networks With Random Access," *IEEE Internet of Things J.*, vol. 9, no. 1, pp. 662–670, Jan. 2022.
- [13] M. Zorzi, "Mobile radio slotted ALOHA with capture, diversity and retransmission control in the presence of shadowing," *Wirel. Netw.*, vol. 4, no. 5, pp. 379–388, 1998.
- [14] M. S. Corson and A. Ephremides, "An analysis of multi-receiver, nonadaptive, slotted ALOHA with capture for wireless communications in factories," in *Proc. IEEE INFOCOM 1993*, San Francisco, CA, USA, Mar. 1993, pp. 421–428.
- [15] Y. Onozato, J. Liu, S. Noguchi, "Stability of a slotted ALOHA system with capture effect," *IEEE Trans. Vehicular Technology*, vol. 38, no. 1, pp. 31–36, 1989.
- [16] A. Gupta and X. Fernando, "Exploring Secure Visible Light Communication in Next-generation (6G) Internet-of-Things," in *Proc. IWCMC 2021*, 2021, pp. 2090–2097.
- [17] S. S. Oyewobi, K. Djouani, and A. M. Kurien, "Visible Light Communications for Internet of Things: Prospects and Approaches, Challenges, Solutions and Future Directions," *Technologies*, vol. 10, no. 1, 2022.
- [18] M. Z. Chowdhury, et al., "The role of optical wireless communication technologies in 5G/6G and IoT solutions: Prospects, directions, and challenges," *Appl. Sci.*, vol. 9, no. 20, 2019.
- [19] A. Hamza and T. Tripp, "Optical wireless communication for the Internet of Things: Advances, challenges, and opportunities," TechRxiv, 18-Jul-2020, doi: 10.36227/techrxiv.12659789.v2.
- [20] M. Haus, et al. "Enhancing indoor IoT communication with visible light and ultrasound," in *Proc. ICC 2019*, Shanghai, China, 2019, pp. 1–6.
- [21] S. R. Teli, S. Zvanovec, and Z. Ghassemlooy, "Optical internet of things within 5G: Applications and challenges," in *Proc. IOTAIIS 2018*, Bali, Indonesia, 2018, pp. 40–45.
- [22] Chia-Wei Chen, et al. "Visible light communications for the implementation of internet-of-things," *Opt. Eng.*, vol. 55, no. 6, 2016.
- [23] Z.-Y. Wu, M. Ismail, E. Serpedin and J. Wang, "Data-Driven Link Assignment With QoS Guarantee in Mobile RF-Optical HetNet of Things," *IEEE Internet of Things J.*, vol. 7, no. 6, pp. 5088–5102, Jun. 2020.
- [24] A. Celik, I. Romdhane, G. Kaddoum, and A. Eltawil, "A Top-Down Survey on Optical Wireless Communications for the Internet of Things," TechRxiv, 17-Jun-2022, <https://doi.org/10.36227/techrxiv.20080580.v1>.
- [25] D. Vukobratovic and F. J. Escribano, "Adaptive multi-receiver coded slotted ALOHA for indoor optical wireless communications," *IEEE Commun. Lett.*, vol. 24, no. 6, pp. 1308 - 1312, June 2020.
- [26] L. Zhao, X. Chi, and W. Shi, "A QoS-driven random access algorithm for MPR-capable VLC system," *IEEE Commun. Lett.*, vol. 20, no. 6, pp. 1239–1242, 2016.
- [27] L. Zhao, X. Chi, and S. Yang, "Optimal aloha-like random access with heterogeneous QoS guarantees for multi-packet reception aided visible light communications," *IEEE Trans. Wireless Commun.*, vol. 15, no. 11, pp. 7872–7884, 2016.
- [28] T. Li, X. Chi, F. Ji, H. Shi, and S. Wang, "Optimal optical camera communication-ALOHA random access algorithm aided visible light communication system," *Opt. Eng.*, vol. 59, no. 7, 2020.
- [29] Y. Polyanskiy, H. V. Poor, and S. Verdú, "Channel coding rate in the finite blocklength regime," *IEEE Trans. Inf. Theory*, vol. 56, no. 5, pp. 2307–2359, May 2010.
- [30] M. Petkovic, T. Devaja, D. Vukobratovic, F. J. Escribano, and Č. Stefanović, "Reliability Analysis of Slotted Aloha with Capture for an OWC-based IoT system", in *Proc. 2021 17th International Symposium On Wireless Communication Systems (ISWCS)*, pp. 1–6, 2021.
- [31] J. M. Kahn and J. R. Barry, "Wireless infrared communications," *Proc. of the IEEE*, vol. 85, no. 2, pp. 265–298, Feb. 1997.
- [32] M. Petkovic, D. Vukobratovic, A. Munari, and F. Clazzer, "Relay-aided slotted aloha for optical wireless communications", in *Proc. CSNDSP 2020*, Porto, Portugal, 2020.
- [33] A. Papoulis and H. Saunders, *Probability, random variables and stochastic processes*, 4th ed., McGraw Hill, 2002.
- [34] I. S. Gradshteyn and I. M. Ryzhik, *Table of Integrals, Series, and Products*. 6th ed., New York: Academic, 2000.
- [35] J. H. Curtiss, "On the distribution of the quotient of two chance variables," *Ann. Math. Stat.*, vol. 12, no. 4, pp. 409–421, 1941.
- [36] J. Scarlett, V. Y. F. Tan, and G. Durisi, "The dispersion of nearest neighbor decoding for additive non-Gaussian channels," *IEEE Trans. Info. Th.*, vol. 63, no. 1, pp. 81–92, Jan. 2017.
- [37] J. Park, "Rate analysis of ultra-reliable low-latency communications in random wireless networks," arXiv, Preprint, arXiv:1910.13868, 2019.